Monitoring Forest Phenology and Leaf Area Index with the Autonomous, Low-Cost Transmittance Sensor PASTiS-57

Benjamin Brede, Jean-Philippe Gastellu-Etchegorry, Nicolas Lauret, Frederic Baret, Jan G. P. W. Clevers, Jan Verbesselt, Martin Herold

remote sensing

MDPI

Article

Monitoring Forest Phenology and Leaf Area Index with the Autonomous, Low-Cost Transmittance Sensor PASTiS-57

Benjamin Brede [1,*], Jean-Philippe Gastellu-Etchegorry [2], Nicolas Lauret [2], Frederic Baret [3], Jan G. P. W. Clevers [1], Jan Verbesselt [1] and Martin Herold [1]

1 Laboratory of Geo-Information Science and Remote Sensing, Wageningen University & Research, Droevendaalsesteeg 3, 6708 PB Wageningen, The Netherlands; jan.clevers@wur.nl (J.G.P.W.C.); jan.verbesselt@wur.nl (J.V.); martin.herold@wur.nl (M.H.)

2 Centre d'Etudes Spatiales de la BIOsphere, Toulouse University, CNES, CNRS, IRD, UPS, (Toulouse), 31401 Toulouse, France; gastellu@cesbio.cnes.fr (J.-P.G.-E.); nicolas.lauret@cesbio.cnes.fr (N.L.)

3 Institut National de la Recherche Agronomique–Université d'Avignon et des Pays du Vaucluse (INRA-UAPV), 228 Route de l'Aérodrome, 84914 Avignon, France; baret@avignon.inra.fr

* Correspondence: benjamin.brede@wur.nl

Received: 15 May 2018; Accepted: 27 June 2018; Published: 30 June 2018

check for updates

Abstract: Land Surface Phenology (LSP) and Leaf Area Index (LAI) are important variables that describe the photosynthetically active phase and capacity of vegetation. Both are derived on the global scale from optical satellite sensors and require robust validation based on in situ sensors at high temporal resolution. This study assesses the PAI Autonomous System from Transmittance Sensors at 57° (PASTiS-57) instrument as a low-cost transmittance sensor for simultaneous monitoring of LSP and LAI in forest ecosystems. In a field experiment, spring leaf flush and autumn senescence in a Dutch beech forest were observed with PASTiS-57 and illumination independent, multi-temporal Terrestrial Laser Scanning (TLS) measurements in five plots. Both time series agreed to less than a day in Start Of Season (SOS) and End Of Season (EOS). LAI magnitude was strongly correlated with a Pearson correlation coefficient of 0.98. PASTiS-57 summer and winter LAI were on average $0.41\,\mathrm{m^2\,m^{-2}}$ and $1.43\,\mathrm{m^2\,m^{-2}}$ lower than TLS. This can be explained by previously reported overestimation of TLS. Additionally, PASTiS-57 was implemented in the Discrete Anisotropic Radiative Transfer (DART) Radiative Transfer Model (RTM) model for sensitivity analysis. This confirmed the robustness of the retrieval with respect to non-structural canopy properties and illumination conditions. Generally, PASTiS-57 fulfilled the CEOS LPV requirement of 20% accuracy in LAI for a wide range of biochemical and illumination conditions for turbid medium canopies. However, canopy non-randomness in discrete tree models led to strong biases. Overall, PASTiS-57 demonstrated the potential of autonomous devices for monitoring of phenology and LAI at daily temporal resolution as required for validation of satellite products that can be derived from ESA Copernicus' optical missions, Sentinel-2 and -3.

Keywords: Land Surface Phenology; Leaf Area Index; ground-based; forest; validation; radiative transfer model; DART model

1. Introduction

Vegetation phenology describes the "timing of seasonal developmental stages in plant life cycles including bud burst, canopy growth, flowering, and senescence [...]" [1]. This includes the start, end and length of the photosynthetically active phase in the year. A mechanistic understanding of controls on these events is still lacking for most biomes [2]. This leads to a general misrepresentation of vegetation temporal behaviour in global circulation models and uncertainty in vegetation-climate feedbacks. Standardised, wide-spread observations are paramount for the quantification of phenology and climate feedbacks.

Proximal sensing techniques such as phenocams or webcams allow high revisit frequency and objective analysis techniques [3–5]. They are based on the principle that changes in canopy biophysical and -chemical composition, which go along with leaf development and senescence, alter its radiative regime. Most often exploited is the decrease of reflectance in the visible wavelengths due to absorption for photosynthesis and the increase in the Near-Infrared (NIR) due to reflecting properties of leaves. The latter effect can be exploited when sensors also record NIR [6,7]. This can be done for example with tower-based proximal sensing. However, these sensors are often not standardised in terms of measurement protocols [8].

Apart from this, the change in reflective behaviour is also utilised to detect phenological events over large areas with satellite-borne sensors [9,10]. The spatially aggregated, temporal behaviour of plants over larger areas that are observed from space is referred to as Land Surface Phenology (LSP) [1]. In contrast to ground-based systems, space-borne missions have the advantage to use only single or few sensors, which makes it easier to derive comparable products.

The case is similar for another quantitative vegetation property, the Leaf Area Index (LAI). It is defined as the one-sided leaf area per unit of ground surface area [11]. Hence, it quantifies the amount of leaves that are available for photosynthesis during the photoperiod. Similar to LSP, LAI can be inferred from ground-based and space-borne instruments, but also from air-borne sensors [12–14] and Unmanned Aerial Vehicless (UAVs) [15,16]. Ground-based LAI observations are typically performed with consumer-grade cameras equipped with fish-eye lenses, referred to as Digital Hemispherical Photography (DHP) [17]. This method relies on gap fraction theory to infer LAI [18]. Most often, observations with a viewing zenith angle of 57.5°, the so-called hinge angle, are analysed, where impact of the Leaf Angle Distribution (LAD) on gap fraction is minimal. Other hand-held instruments are also available. However, in general, ground-based instruments for LAI are used manually and in campaigns that cover larger areas to capture the extent of satellite scenes [13]. Regular re-sampling of the same locations is possible, but labour-intensive [19,20].

In the context of Earth observation satellite missions and programmes, such as NASA's Moderate-Resolution Imaging Spectroradiometer (MODIS) or ESA's Sentinel-3 mission [21,22], both LSP and LAI spatial products require robust quality ground-based validation. This demands monitoring devices that match land product's temporal resolution, potentially able to record LAI at high resolution so that LSP can be inferred from the time series. Low-cost devices would be preferred to allow deployment over larger areas and at many sites.

The PAI Autonomous System from Transmittance Sensors at 57° (PASTiS-57) is a candidate to fulfil these requirements. It was developed by Institut national de la recherche agronomique (INRA)-Hiphen (Avignon, France) during the FP7 ImagineS project (http://fp7-imagines.eu). Its main application was to support multi-day calibration and validation field campaigns for retrieval of LAI and Fraction of Absorbed Photosynthetically-Active Radiation (FAPAR) with hectometric resolution space-borne sensors [23–26]. Recently, it was compared with seasonal measurements of LAI-2200 and DHP in agricultural fields [27]. Its measurement principle is based on gap fraction theory. Similar to DHP, it exploits the LAD quasi-invariance at the hinge angle. However, a more detailed assessment of its performance characteristics especially with respect to changing illumination conditions and plant biochemical properties has not been presented yet.

In this context, vegetation Radiative Transfer Models (RTMs) can support sensitivity analysis, the definition of new sensors and the development of inversion procedures to translate the radiative signal into canopy variables [28]. Generally, vegetation RTMs model the interaction of sun radiation with canopy elements based on the canopy's biophysical and -chemical properties. In this way, they can be exploited to assess the sensors sensitivity to canopy parameters in idealised conditions, i.e., without measurement noise, and for a wide range of possible canopy conditions. For example, the widely used PROSAIL model, a combination of the Scattering by Arbitrarily Inclined Leaves (SAIL) canopy and PROSPECT leaf radiative models, has been exploited to design vegetation indices [29] and for biophysical parameter retrieval via inversion [30–32]. However, SAIL represents the canopy as a homogeneous layer of scatterers. This assumption does not hold for clumped canopies such as forests.

In these cases, a heterogeneous representation that can take into account canopy clumping and non-random structure is more appropriate. The Discrete Anisotropic Radiative Transfer (DART) model implements this paradigm [33]. DART applications include canopy biophysical and -chemical parameter retrieval [34,35], surface energy budget studies [36] and recently chlorophyll fluorescence modelling [37]. Additionally, DART incorporates the option to implement in-scene sensors such as hemispherical or pinhole cameras [37]. This provides the option to test arbitrary sensor designs.

The aim of this study has been twofold: (i) testing the ground-based transmittance sensor PASTiS-57 for monitoring LSP and LAI in a forest stand with daily frequency; and (ii) assessing the sensor's sensitivity to canopy properties other than LAI and their interactions by means of RTM experiments, thereby testing the robustness of the measurement principle to different canopy conditions. This study is structured as follows: The PASTiS-57 sensor is presented in detail in Section 2.1. Section 2.2 describes the field data collection and analysis. Section 2.3 elaborates on implementation of the sensor in DART, the set up of the synthetic canopy and how sensitivity analysis was conducted. Results are presented in Section 3 and discussed in Section 4. Section 5 summarises the results and lists implications for future sensor design.

2. Materials and Methods

2.1. PASTiS-57 Instrument

The PASTiS-57 consists of a weather proof, battery powered datalogger with 6 photodiode-based sensors (Figure 1). The sensors are fixed to a viewing zenith angle of 57.5°, sensitive in the blue spectral region to minimise canopy multiple scattering and have different lengths of wire for sensor distribution around the data-logger. The logger is battery powered and can autonomously collect data at 1 min interval for up to four months. Intervals of 2 min and 5 min are also possible. Radiation is recorded with uncalibrated Digital Number (DN) in the interval 0–4000, whereas larger DNs are treated as unreliable due to saturation effects. The signal can be calibrated with dedicated Photosynthetically-Active Radiation (PAR) sensors [25]. However, a more practical approach is to utilise the relative signal by installing one device above the canopy, which serves as reference for incoming radiation, and another device below the canopy, which represents the observations. In this way, many plots can be served by one reference sensor, as long as it is within a distance where illumination conditions can be assumed comparable. The observed signal is the spectral directional transmittance τ for each sensor:

$$\tau = \frac{DN_{below\ canopy}}{DN_{above\ canopy}} \tag{1}$$

2.2. Field Experiment

2.2.1. Study Area and Field Data Collection

PASTiS-57 sensors have been installed at the Speulderbos Fiducial Reference site in the Veluwe forest area (N52°15.15′ E5°42.00′), The Netherlands [38] (www.wur.eu/fbprv). This site represents a maturing stand of mixed European beech (*Fagus sylvatica*), pedunculate oak (*Quercus robur*) and sessile oak (*Quercus petraea*) with few understorey. The trees were initially planted in 1835. Nowadays, the stand has a density of around 200 trees/ha.

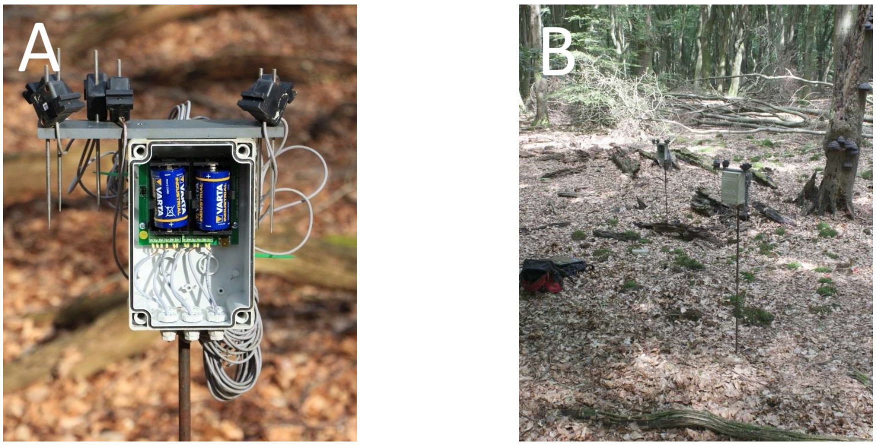

Figure 1. The PASTiS-57 instrument installed in the Speulderbos site: (**A**) With the opened data-logger box, the six sensors can be seen on top, a spare cable is curled up at the back of the data-logger, and two D-cell batteries for power supply in the box; and (**B**) two PASTiS-57 installed at the centre of Plot C (centre marker not visible).

PASTiS-57 instruments were installed in the centres of five plots. For redundancy, each plot was equipped with two devices (Figure 2). Contrary to previous studies where sensors were put onto the ground, the individual sensors in this study have been mounted on top of the data logger on a plastic board to face the NE, E, SE, SW, W and NW directions. Each PASTiS-57 unit was fixed at 1.30 m above ground at an iron rod, aligned to north with a magnetic compass and levelled with a bubble level. Another two devices have been mounted at the top of a 42 m high scaffold tower approximately 550 m west of Plot A to record above canopy reference downward radiation. Campaigns were conducted in spring 2016 during leaf flush, autumn 2016 during leaf senescence, and summer and autumn 2017. Campaigns were programmed with 2 min interval in 2016 and 1 min interval in 2017.

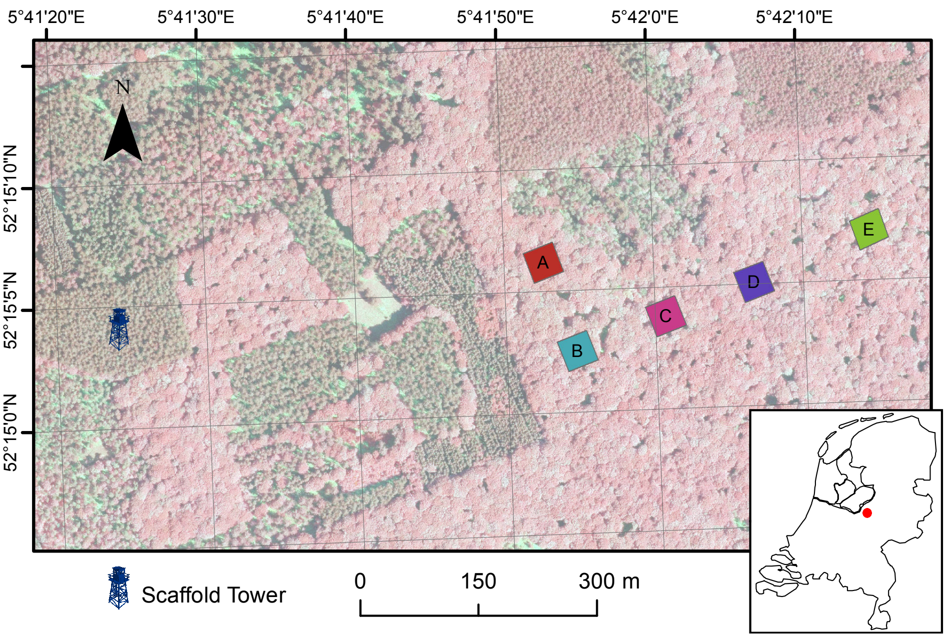

Figure 2. Map of the study site with the scaffold tower where reference instruments were placed and the five sampling plots. Background is an airborne false-colour composite of 2013. The location of the study site within The Netherlands is marked on the inset.

2.2.2. Plant Area Index (PAI) Retrieval

It should be noted that many proximal sensing techniques cannot distinguish between foliage and woody canopy elements. The PAI includes both classes, while LAI refers only to photosynthetically active plant tissue [39,40]. In the following, PAI refers to observed plant area, while LAI refers to the actual quantity of green leaf area. Typically, LAI retrieval from below canopy sensors such as DHP uses gap fraction theory [18,41]. For this, the canopy is assumed as a uniform cloud of randomly oriented, black facets ($\rho = 0$, $\tau = 0$). In this case, the gap fraction is related to LAI based on Beer–Lambert's law:

$$P(\theta) = e^{-G(\theta)\Omega(\theta)L/\cos\theta} \tag{2}$$

where θ is the viewing zenith angle, $P(\theta)$ the canopy gap fraction in direction θ, $G(\theta)$ the projection of unit foliage in the θ direction, which characterizes the foliage angular distribution, $\Omega(\theta)$ the clumping index that describes the non-randomness of the canopy and L the LAI. $P(\theta)$ has been variably interpreted as gap fraction in the case of DHP [18], hit probability in the case of lidar sensors [42,43] or transmittance in the case of PASTiS-57 [24,26].

For canopy clumping estimation, the method of Lang and Xiang (LX) [44] and the six different viewing directions of each PASTiS-57 instrument were exploited. The LX method assumes that within a segment the foliage is random and it contains gaps. In the case of PASTiS-57 the instantaneous field of view of a single sensor can be interpreted as a segment. In that case, canopy clumping can be described as:

$$\Omega(\theta) = \frac{\ln \overline{P(\theta)}}{\overline{\ln P(\theta)}} \tag{3}$$

where $\overline{P(\theta)}$ is the mean gap fraction of all segments and $\overline{\ln P(\theta)}$ the logarithm of the mean gap fraction of all segments. "The reasoning behind this technique is that since the [LAI] is related to the natural logarithm of the gap fraction, the average LAI should follow the logarithm average of the gap fraction" [41]. In this sense, the denominator in Equation (3) normalises the gap fraction by the logarithm. Using this definition for clumping, replacing $P(\theta)$ with PASTiS-57 measured transmittance τ_{PASTIS} and exploiting the near constant value of the G-function at $\theta = 57.5°$ for many LAD reduces Equation (2) to

$$L = \frac{-1.075\ln(\tau_{PASTIS})}{\Omega} \tag{4}$$

The goal of this study was to produce daily observations of LAI, from which phenological parameters can be derived. Earlier studies in forests showed that sub-daily retrievals with PASTiS-57 based on Equation (4) produce results with strong, high frequency noise with ± 0.5 LAI amplitude [45]. Therefore, raw readings require appropriate quality filters to be applied. Here, these filters were based on experience gathered while investigating the raw time series. The primary result was that high frequency noise stems from changing illumination conditions that violate the assumptions for the retrieval.

Firstly, broken cloud cover can result in different sky illumination conditions at the location of the reference and the observation sensors. Here, this was counteracted by aggregating via averaging of the 1 min transmission readings to a daily time series. Secondly, strong cloudiness reduces the radiation reaching the forest floor, especially at the north-facing sensors, resulting in below canopy DN of 0, which are interpreted as infinite PAI (Equation (4)) and do not match the assumptions behind the clumping appraisal. Therefore, DN readings of 0 for the below canopy sensors were removed from the time series. Thirdly, large canopy gaps result in direct illumination on the below canopy sensor, which violates the assumption of diffuse illumination and produces high DN readings. These conditions are only of short duration when the sun moves over the specific gap. Even the NW and NE sensors experience these conditions when canopy elements are overly strong illuminated through canopy gaps and result in recorded high transmission. To counteract this effect, all DN exceeding the 95th daily percentile were removed.

2.2.3. Reference Datasets

Next to PASTiS-57 records, a multi-temporal campaign with a RIEGL VZ-400 Terrestrial Laser Scanning (TLS) (RIEGL LMS GmbH, Horn, Austria) was conducted at the Speulderbos site. This scanner has shown good results for monitoring phenology [39]. The main advantage of TLS as a gap fraction sensor is its independence from illumination conditions [42,46,47]. This results in high precision time series, i.e., with low noise in the temporal domain. On the other side, partial hits lead to underestimation of gap fraction by these kind of sensors [46,48]. Partial hits result from objects that only partially cover the laser instantaneous field of view, but are registered as full interceptions by the waveform analysis methods of commercial suppliers to maximise point cloud density. In this way, gap fraction is underestimated and, consequently, PAI is overestimated. In addition, wet canopy conditions have to be avoided for the sampling, because water droplets on canopy elements absorb the laser beam, thereby apparently increasing gap fraction.

In total 45 sampling events were conducted. The sampling strategy was to focus efforts during change periods, i.e., Start Of Season (SOS) and End Of Season (EOS), and to avoid rain conditions. For each sampling event, the scanner was mounted on a surveying tripod in each centre of the five plots, at a maximum distance of 3 m from the respective PASTiS-57 devices. $P(\theta)$ was derived from the hemispherical scans by taking into account the multi-return capability of the scanner [43]. The hinge angle was approximated with the 55° to 60° region, which is a typical strategy [39,42,43].

Apart from the ground-based TLS time series, MODIS Collection 6 MCD15A3H LAI products were retrieved [49,50]. MCD15A3H is a four-day composite product based on inversion of a vegetation RTM. Its eight-day companion product was validated to Stage 2 according to the Land Product Validation (LPV) subgroup (https://lpvs.gsfc.nasa.gov/). However, the four-day product was preferred over the eight-day product as the goal here included estimating temporal metrics, thus denser samples were important.

The samples were retrieved from the Application for Extracting and Exploring Analysis Ready Samples (APPEARS) service of the US Geological Survey (https://lpdaacsvc.cr.usgs.gov/appeears/) for the period 1 January 2016 until 28 February 2018 and for the 500 m pixel centred at the Speulderbos site. This means that the MCD15A3H samples also included forest patches other than beech, e.g., some mixed species stand included in the Speulderbos site. After downloading, the time series was filtered with the accompanying quality flags to allow only good quality LAI retrievals. After visual inspection it was clear that some outliers in summer with LAI below $3\,\mathrm{m^2\,m^{-2}}$ occurred, which have been excluded as well.

2.2.4. Phenological Model Fitting

LSP can be modelled with logistic functions [1,9]. These mathematically simple models are fitted piecewise to time series of vegetation indices or LAI to describe the spring growth and autumn senescence periods [39]. From these models LSP indicators like SOS and EOS can be derived. Here, a logistic model was used [9,39]:

$$PAI(t) = \frac{U - L}{1 + e^{-k(t - t_m)}} + L \tag{5}$$

where t is time (expressed as Day Of Year (DOY)), U the upper asymptote ($\mathrm{m^2\,m^{-2}}$), L the lower asymptote ($\mathrm{m^2\,m^{-2}}$), k the growth rate ($\mathrm{d^{-1}}$) and t_m the inflection point, where k is maximal (DOY). The model was fitted with a non-linear least squares routine implemented in the `nls` function of the R `stats` package [51,52]. Separate sigmoids were estimated for the spring 2016 and autumn 2017 periods. In addition to the model parameters' best estimates, non-linear least squares estimate also produces prediction intervals. Finally, SOS and EOS were estimated as the time of the year when the fitted model reached the 95% upper and lower prediction interval for the L and U parameter, respectively.

This fitting strategy was applied separately to the PASTiS-57, TLS and MODIS time series, and results were compared.

2.3. Radiative Transfer Model Experiments

In-scene sensors in DART can be implemented as frame cameras with arbitrary viewing direction and properties (see Figure 3 for an example), and record at-sensor spectral radiance for any number of spectral bands with any bandwidths ($\mathrm{W\,m^{-2}\,sr^{-1}\,\mu m^{-1}}$). For this study, the frame camera characteristic was not exploited, but only the integrated radiance over the whole sensor FOV was regarded similar to the PASTiS-57 photo-diodes. As in the field set up (Section 2.2), in this simulation the 6 PASTiS-57 sensors were directed in the NE, E, SE, SW, W and NW directions with a viewing zenith angle of 57.5°. In the DART scene, one device consisting of six sensors was positioned below, another above the simulated canopy, so that canopy transmittance could be calculated in the same way as in the field experiment (Equation (1)). The PASTiS-57 spectral response curve is not exactly known, so a blue waveband centred at 490 nm with 20 nm bandwidth (FWHM) was chosen. Additionally, bands centred in the green (560 nm), red (665 nm) and NIR (865 nm) were tested following the specifications of the Sentinel-2 Multi Spectral Instrument (MSI) [53]. These additional bands allowed judging the instrument performance in the case photo-diodes would have been chosen that are sensitive in another spectral region.

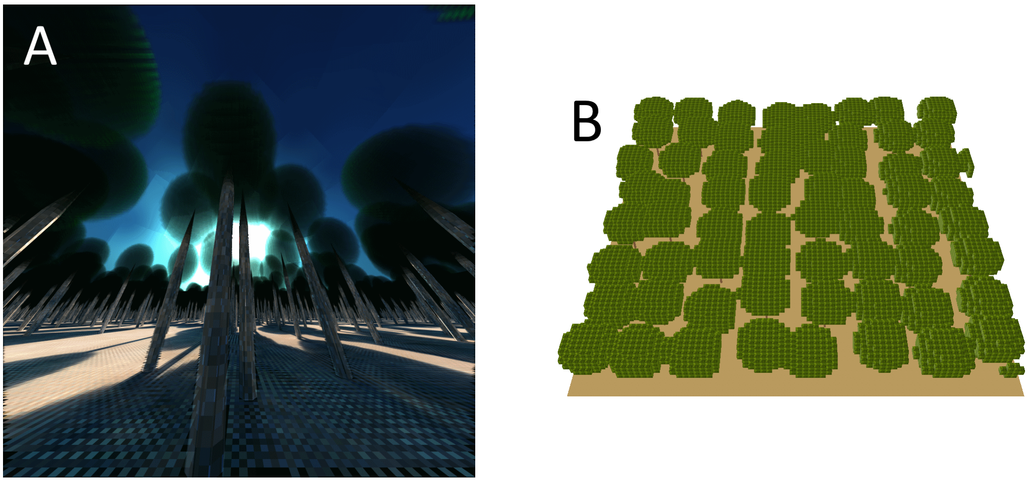

Figure 3. DART sample scene: (**A**) True colour image sample for below-canopy sensor in DART. The viewing zenith angle is 57.5°, but the field of view is extended compared to the sensors used in the modelling to give an overview of the scene. (**B**) Top view of the created mock-up with 50 trees.

Two scenarios were set up to test different canopy parameters. In both, only the sensitivity of PASTiS-57 to change in LAI was investigated, but not to the temporal evolution. This is justified with the direct dependence of temporal sensitivity on the sensitivity to LAI. The first scenario modelled the canopy as a turbid medium, which is in accordance to gap fraction theory that is underlying the LAI retrieval (Section 2.2.2). This scenario was intended to test the retrieval robustness to different illumination conditions as well as variation in biophysical and -chemical canopy composition. Table 1 summarises the parameters and their chosen values. For each case, one typical and two extreme cases were chosen. All parameters were varied in a full grid approach, resulting in a total of 450 simulations. For this experiment, clumping was not investigated ($\Omega = 1$) because the canopy was homogeneous in all directions. The solar azimuth angle was kept constant at 180°. The simulated sensors were analysed with respect to their prediction performance of the true LAI. The results were compared with the Global Climate Observing System (GCOS) requirement for LAI retrieval accuracy, which is 20% as well as the accuracy goal for agricultural meteorology applications identified by the WMO , which is 5% [54]. The Relative Error (RE) was chosen as accuracy metric and calculated as:

$$RE = \frac{PAI_{simulated\ PASTIS} - LAI_{DART}}{LAI_{DART}} \tag{6}$$

where LAI_{DART} is the DART input LAI and $PAI_{simulated\ PASTIS}$ the PAI derived with the simulated PASTiS-57. Using this formulation, positive REs meant overestimation of the PASTiS-57-derived PAI.

During analysis of the results of these RTM simulations, a systematic bias in PAI estimation has been identified. This could be linearly modelled with the form $PAI = aLAI + b + \epsilon$ independently for each LAD ($p < 0.01$). For assessment of this error's impact on LSP metrics estimation, PAI in Equation (5) was replaced with the linear bias model and solved for t. The comparison of this with the unbiased estimation of t gave the expected error in LSP metric. Since the analytic solution was complex, the impact of the relative error was assessed numerically by testing a range of values for U, L and k. In the case of U and L extreme combinations were tested, i.e., $L = 0$ and $U \in \{1, 2, ...10\}$. In the case of k, estimates from the field derived models were used (Section 2.2.4), i.e., $k \in \{0.5, -0.08\}$. Values for t_m were not necessary, because it cancels out when only considering the difference between two estimates.

Table 1. Biophysical, biochemical and illumination parameters and values used for turbid DART experiments.

Parameter	Values	Unit
Leaf Area Index (LAI)	1, 2, ..., 10	$m^2\,m^{-2}$
Leaf Angle Distribution (LAD)	spherical, erectrophile, planophile, extremophile, plagiophile	-
Chlorophyll a and b (C_{ab})	20, 50, 80	$\mu g\,cm^{-2}$
Solar Zenith Angle (SZA)	0, 57.5, 80	$^\circ$

The second scenario was intended to test the retrieval performance with respect to canopy non-randomness. For this, discrete trees were modelled with ellipsoid crowns with 10 m diameter and 5 m height, and trunks with 40 cm diameter. The number of trees per scene was varied between 50 and 400 trees on a scene of 80 m × 80 m. Illumination and canopy biochemical parameters were held constant with a spherical LAD, 50 $\mu g\,cm^{-2}$ C_{ab} and SZA of 57° to extract the effect of clumping alone.

3. Results

3.1. Field Experiment

Figure 4 shows the raw DN recordings of two sampling days, one before SOS, one after leaf flush in summer. For both days, averages were clearly lower than reference readings above the canopy, resulting in average canopy transmittance of 29.1% and 0.9% before and after the start of season, respectively. Another feature was the high number of 0 DN readings at early and late hours of the day after leaf flush, which made up 25.7% of all observations on that day. At these times, the SZA is typically large, so that the direct path through the canopy is long and not sufficient radiation reaches the below canopy sensors. In contrast to this, the SW sensor on the reference device experienced saturation in the afternoon, probably due to direct illumination. Overall, the two days showed high agreement in temporal evolution, indicating similar impact of changes in illumination. These stem from the course of the sun, resulting in the rise and fall of readings over the course of the day, and from clouds and stems, causing high frequency changes.

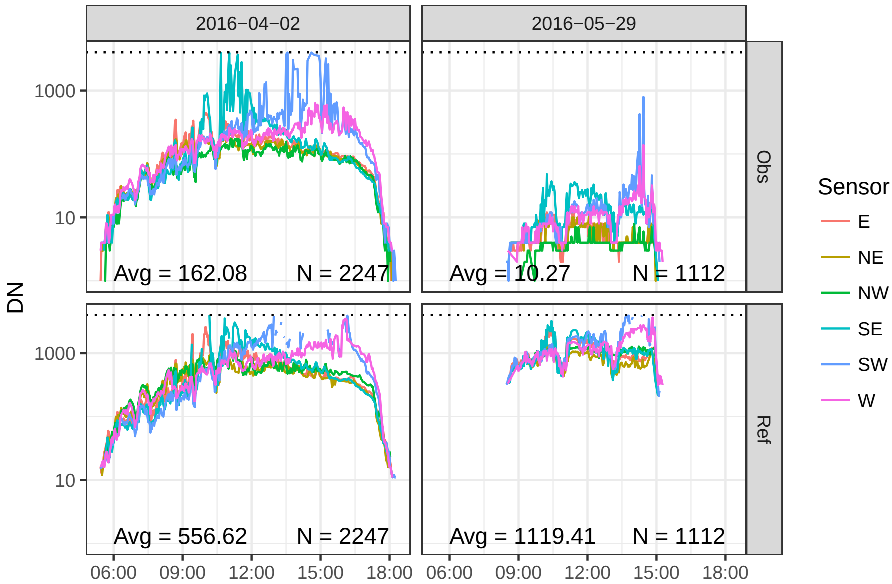

Figure 4. Recordings of two sampling days for one device in Plot A. Upper panels are the observations below the canopy, lower panels are reference readings from above the canopy. DN axis is on log-scale. Dotted horizontal line is saturation point at 4000 DN. Discontinued lines on lower panel reach saturation. Only pairs for which the observation did not reach 0 Digital Number were considered.

A full PAI time series for all three campaigns derived from a device on Plot C can be seen in Figure 5. While the difference between the single sensors was only marginal, the impact of the filtering was clearly visible. The naive retrieval resulted in strong, high frequency noise with positive spikes and a Lag 1 Auto-Correlation Coefficient (ACC1) of 0.93. The noise after filtering was modest and evolved equally around a mean course of PAI with ACC1 of 0.97. The former resulted from situations under full canopy in summer, when the below-canopy sensors had 0 DN readings. This results in theoretically infinite PAI according to Equation (4). When comparing the two years, an earlier decrease in PAI could be observed in 2017. This can be explained with the natural variability of EOS. This results from different wind loads, which is the main force to defoliate the trees once the leaves have died.

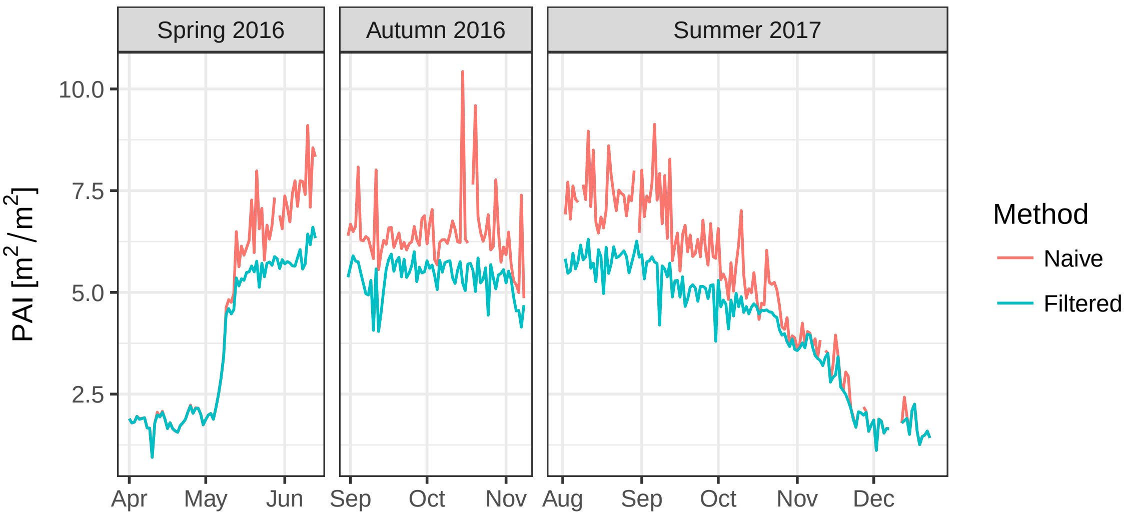

Figure 5. All campaigns of one instrument in Plot C before (Naive) and after application of filtering (Filtered).

In Figure 6 PASTiS-57 and TLS estimated PAI are plotted together for the dynamic phases of the yearly phenology, which are spring leaf flush and autumn senescence. Overall, PASTiS-57 and TLS showed high agreement in temporal development. Both sensors' time series reflect the fast leaf development during spring and the longer senescence period in autumn. The TLS sampling intervals were not sufficient to record the fast changes in spring, especially between the sampling events of 4 May 2016 and 12 May 2016 when PAI increased by $1.86\,\mathrm{m^2\,m^{-2}}$ on average within eight days. The PASTiS-57 with their daily interval could closely follow the development.

Considering the magnitude, both sensors agreed strongly with a Pearson correlation coefficient of 0.98. However, PASTiS-57 retrievals were lower in winter by $1.44\,\mathrm{m^2\,m^{-2}}$ compared to TLS. This was likely due to the different sensing techniques. In case of PASTiS-57, backward scattering from woody elements increases recorded radiation at the below canopy sensors, thus decreases PAI estimates. In the case of TLS, the partial hits are mainly responsible for the sensitivity to the recording of canopy elements. For both instruments, PAI > 1.5 in winter pointed to the large influence of woody material on the retrievals. In contrast to this, PASTiS-57 average and TLS agreed in summer to within $0.74\,\mathrm{m^2\,m^{-2}}$.

Parameter estimates for the fitted phenological models are summarised in Tables 2 and 3. A total of 21 and 40 samples for each plot were used for TLS and MODIS, respectively. Concerning the upper and lower asymptotes U and L, PASTiS-57 showed significantly lower estimates compared to TLS in all plots. For both spring and autumn campaigns, PASTiS-57 U and L were on average $0.41\,\mathrm{m^2\,m^{-2}}$ and $1.43\,\mathrm{m^2\,m^{-2}}$ lower than TLS, reflecting the difference in acquisition mechanism. Compared to MODIS, PASTiS-57 U and L were $0.19\,\mathrm{m^2\,m^{-2}}$ lower and $0.97\,\mathrm{m^2\,m^{-2}}$ higher, respectively. Again, this reflects the different nature of the retrieval algorithms. MODIS LAI makes use of top of canopy reflectance and is stronger utilising the NIR signal. This makes it less sensitive to woody material in the canopy, thus MODIS LAI showed generally lower values than PASTiS-57.

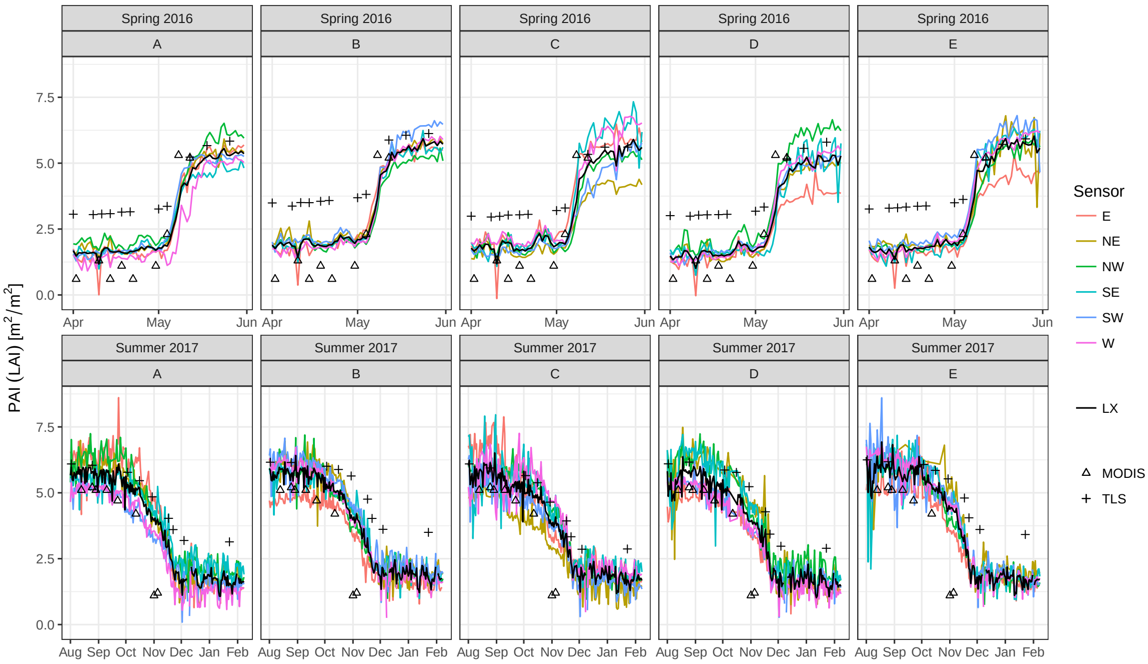

Figure 6. Comparison of PASTiS-57 and TLS derived PAI for single sensors (coloured) and Land and Xiang clumping correction (LX), and MODIS LAI for five plots during the spring 2016 and summer 2017 campaigns.

Table 2. Phenological model fitting results for the spring 2016 campaign with parameter mean estimates and their 95% standard error. U is the upper asymptote ($m^2 m^{-2}$), L the lower asymptote ($m^2 m^{-2}$), k the growth rate (d^{-1}), t_m the inflection point (DOY) and SOS the Start Of Season (DOY). MODIS results refer to all plots and represent LAI in case of U and L.

Parameter	A	B	C	D	E
U_{PASTIS}	5.31 (±0.04)	5.65 (±0.04)	5.46 (±0.05)	5.09 (±0.05)	5.67 (±0.05)
U_{TLS}	5.82 (±0.03)	6.10 (±0.03)	5.72 (±0.04)	5.62 (±0.04)	5.99 (±0.03)
U_{MODIS}	5.63 (±0.15)	–	–	–	–
L_{PASTIS}	1.63 (±0.03)	1.94 (±0.03)	1.85 (±0.04)	1.57 (±0.03)	1.75 (±0.04)
L_{TLS}	3.10 (±0.02)	3.51 (±0.03)	3.02 (±0.03)	3.03 (±0.03)	3.32 (±0.02)
L_{MODIS}	0.80 (±0.09)	–	–	–	–
k_{PASTIS}	0.43 (±0.03)	0.49 (±0.04)	0.54 (±0.06)	0.48 (±0.04)	0.44 (±0.03)
k_{TLS}	0.41 (±0.03)	0.52 (±0.05)	0.47 (±0.04)	0.43 (±0.04)	0.31 (±0.02)
k_{MODIS}	0.77 (±0.26)	–	–	–	–
$t_{m,PASTIS}$	129.5 (±0.2)	129.3 (±0.2)	129.3 (±0.2)	129.2 (±0.2)	129.1 (±0.2)
$t_{m,TLS}$	130.0 (±0.3)	128.6 (±0.4)	129.3 (±0.4)	129.5 (±0.4)	130.9 (±0.3)
$t_{m,MODIS}$	126.0 (±0.5)	–	–	–	–
SOS_{PASTIS}	117.9	119.5	121.0	119.6	118.4
SOS_{TLS}	118.2	119.9	119.7	119.2	115.8
SOS_{MODIS}	120.9	–	–	–	–

Table 3. Same as Table 2, but for the autumn 2017 campaign referring to the EOS (DOY).

Parameter	A	B	C	D	E
U_{PASTIS}	5.69 (±0.04)	5.72 (±0.03)	5.64 (±0.05)	5.49 (±0.05)	5.79 (±0.04)
U_{TLS}	6.06 (±0.08)	6.07 (±0.08)	6.00 (±0.13)	6.05 (±0.12)	6.15 (±0.10)
U_{MODIS}	5.06 (±0.11)	–	–	–	–
L_{PASTIS}	1.59 (±0.04)	1.80 (±0.04)	1.69 (±0.05)	1.55 (±0.05)	1.64 (±0.04)
L_{TLS}	3.05 (±0.10)	3.43 (±0.14)	2.74 (±0.17)	2.78 (±0.18)	3.34 (±0.16)
L_{MODIS}	0.65 (±0.09)	–	–	–	–
k_{PASTIS}	−0.08 (±0.00)	−0.08 (±0.00)	−0.07 (±0.00)	−0.08 (±0.01)	−0.09 (±0.01)
k_{TLS}	−0.08 (±0.01)	−0.12 (±0.02)	−0.07 (±0.01)	−0.10 (±0.02)	−0.09 (±0.02)
k_{MODIS}	−0.16 (±0.02)	–	–	–	–
$t_{m,PASTIS}$	307.6 (±0.7)	307.8 (±0.7)	307.5 (±1.0)	309.8 (±1.0)	311.7 (±0.7)
$t_{m,TLS}$	307.2 (±1.9)	317.4 (±2.0)	307.4 (±3.0)	314.4 (±2.6)	316.7 (±2.6)
$t_{m,MODIS}$	292.5 (±1.7)	–	–	–	–
EOS_{PASTIS}	250.0	250.4	243.2	256.2	262.8
EOS_{TLS}	258.8	288.4	263.7	280.8	281.4
EOS_{MODIS}	269.0	–	–	–	–

Furthermore, PASTiS-57 agreed very well with TLS in terms of SOS with an average difference of less than a day. EOS was estimated on average 22 days later by TLS. However, agreement among TLS plots was low with a range of 29 days in EOS. More samples during winter would have been necessary to decrease the estimation error. Moreover, PASTiS-57 achieved the lowest estimation standard error on the sigmoid inflection points t_m. This was made possible by the high temporal density of the PASTiS-57 time series. Additionally, PASTiS-57 agreed well with MODIS SOS to within 2 days. As in the case of TLS, EOS estimation of MODIS was impaired. Only for MODIS, persistent cloud cover—which is common in autumn in The Netherlands—prevented frequent observations.

3.2. Radiative Transfer Model Experiments

The DART RTM experiments permitted to have control over all canopy and illumination parameters, and to model abstract canopies. Figure 7 summarises the results for the turbid medium canopy case. Most influential was the choice of the spectral band. For instance, NIR retrievals were generally more than 75% lower than true LAI. This strong misinterpretation stems from the retrieval assumption of black leaves, which is not fulfilled in the NIR. In fact, leaves typically transmit around 45% of incoming radiation in this band. This leads to higher recorded radiation below canopy and underestimation of LAI. Additionally, the RE was larger at small SZA. This could be explained by a smaller optical path through the canopy at small SZA, which leads to increased below-canopy recorded radiation compared to what would be expected for black leaves. These effects could also be observed to some degree in the green spectral band, where leaves typically transmit >10%.

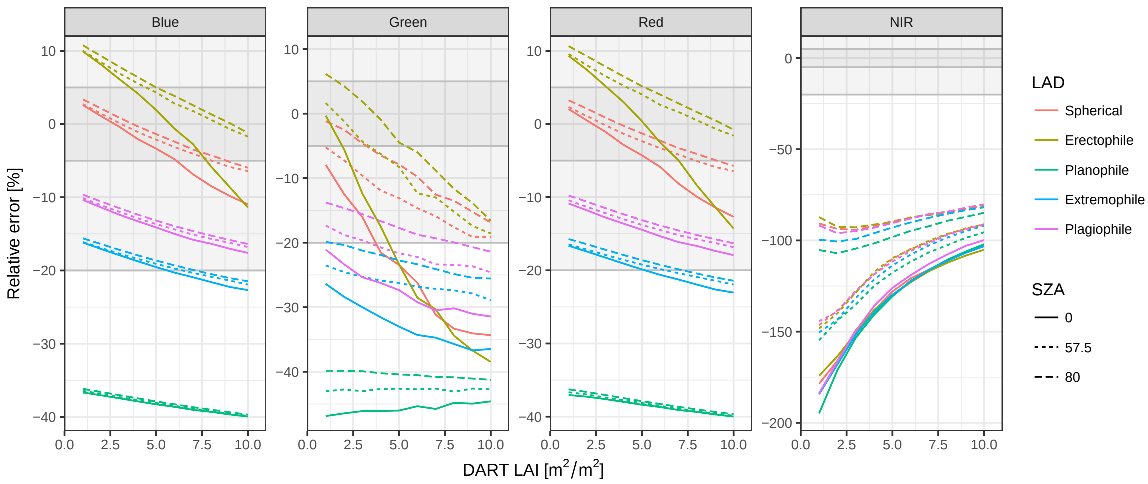

Figure 7. DART model results for turbid canopy representation for west facing sensors. Positive errors mean over-estimation by the retrieval. Light grey and darker grey areas are the 20% and 5% accuracy requirement of GCOS [54].

In contrast, the blue and red bands were less compromised. They both underestimated true LAI by maximum 40.0% and on average by 14.2% and 14.5%, respectively. Thus, the average accuracy was within the GCOS threshold accuracy of 20%. Leaf absorption is strongest at these wavelengths due to absorption by chlorophyll, so that the canopy comes close to the approximation of black facets. Typical transmittance for these spectral regions is <2% and reflectance <4%. This is why blue channels of digital cameras are recommended for LAI retrieval [20,55]. Nonetheless, even these low values in ρ and τ led to higher detected radiation at the sensor compared to what would be expected with black leaves, so that canopy transmittance was overestimated, which leads to underestimation of PAI.

Within the blue and red spectral bands most variation was across the different LADs. While the spherical LAD underestimated true LAI by an average of 2.8% and a maximum of 11.0% in the blue, simulated canopies with planophile LADs resulted in average and maximum underestimation of 38.2% and 40.0%, respectively. In the latter case, the deviation of the *G*-function value from 0.5 and transmitting properties of the leaves probably interacted to increase the deviation from true LAI.

Apart from this, underestimation was generally increasing with true LAI. This means that at higher LAI more radiation was reaching the sensor than expected by the model, i.e., canopy transmittance is larger than expected. This effect could be created by multiple scattering in the canopy. According to the model assumption there are no scattering processes within the canopy. Radiation is only absorbed or transmitted without interaction. However, the DART simulated leaves had $\tau > 0$, which allows radiation to go through leaves. The more leaves there are, the stronger the mismatch between gap fraction and DART model.

Concerning C_{ab}, pairwise Student's t-tests between any of the C_{ab} levels showed no significant differences in LAI estimation ($p > 0.95$) and differences were below 0.1%. This showed that the direct influence of C_{ab} on LAI estimation was very low.

Finally, SZA had minor overall impact on the retrievals. This was on average 0.9% in the blue band between SZA 0° and 57.5°. However, the difference was larger for spherical and erectophile LADs. The extreme case was at LAI 10, where the relative error for 0° and 57.5° differed by 5.1° and 9.7° for spherical and erectophile LADs, respectively.

When translating the impact of the bias in LAI retrieval on LSP metrics, erectophile LADs delivered the largest error with 1.9 days later estimation of EOS. Spherical, planophile, extremophile and plagiophile LADs resulted in 1.5 days, 0.8 days, 1.0 days and 1.1 days later EOS, respectively. SOS estimation showed lower errors with on average 0.1 days. This means EOS as the generally slower process experiences larger errors in LSP metric retrieval based on the LAI bias error. It should be noted that this difference was based on the particular phenological model used here (Section 2.2.4), but models based on sigmoid functions in general should experience errors on the same order of magnitude.

RTM results for the heterogeneous scenario are presented in Figure 8. Tree density was significantly altering retrieval performance in scenarios with <200 trees and LAI > 5 m^2 m^{-2}. This led to underestimation of up to 69.4% at true LAI 10 m^2 m^{-2} and a scene with 50 trees. For these scenarios the present leaf mass was concentrated in few crowns, so that the assumption of a homogeneous canopy did not hold and LAI was underestimated. The clumping correction after Lang and Xiang [44] could account for some of these effects, but could only reduce the underestimation to 55.1% in the case of 50 trees. In those cases, the assumption of a random foliage distribution within the sensor FOV was violated. Actually, the horizontal FOV of the PASTiS-57 is large compared to the solid angles that camera pixels represent. The clumping correction after Lang and Xiang [44] corresponds rather to the small FOVs represented by camera pixels.

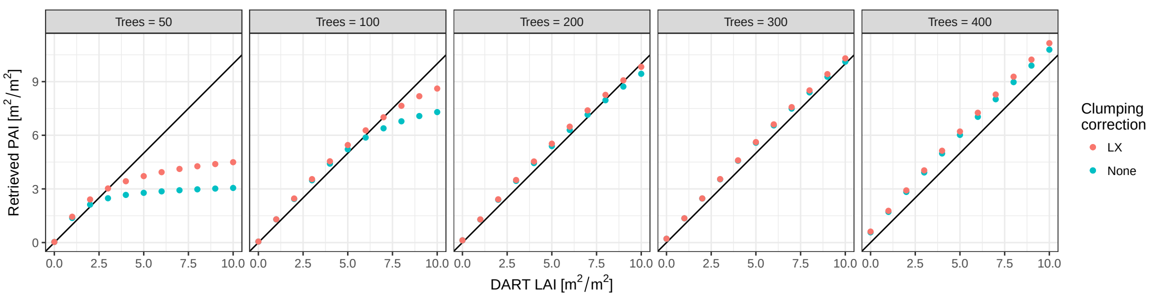

Figure 8. DART model results of discrete canopy representation for five different tree densities (horizontal panels in number of trees). Retrieval without (None) and with clumping correction after Lang and Xiang (LX) [44].

4. Discussion

Ground-validation of LSP and LAI require high temporal density canopy observations. This study explored the PASTiS-57 instrument for autonomous monitoring of phenology and PAI in a Dutch beech forest. DART RTM experiments helped to evaluate sensing mechanism of the PASTiS-57 in relation to changes in canopy biochemical and structural properties other than LAI.

The field experiments showed very good temporal agreement with illumination independent TLS and MODIS LAI products when temporal density of these reference products was high. Biases in PAI magnitude were attributed to differences in sensing mechanism. The field observations required filtering and aggregating the readings to daily time series to reduce high frequency noise, especially during full canopy coverage in summer. This noise can be partially tracked back to the sensor's radiometric resolution of 4000 DN. Considering Equation (4), the change in PAI per DN, which is the sensitivity to signal digitisation, is inversely proportional to the DN. This is because the first derivative of Equation (4) with respect to τ is proportional to the inverse of τ: $L' \propto -\frac{1}{\tau}$. This can result in differences as large as $0.75\,\mathrm{m}^2\,\mathrm{m}^{-2}$ between DN observation readings of 1 and 2 when the reference sensor is close to saturation (Figure 9). Radiometric sensitivity also impacts the maximum PAI that can be recorded. In the case of PASTiS-57, it lies at $8.91\,\mathrm{m}^2\,\mathrm{m}^{-2}$ with a single measurement. Modern digital cameras typically offer digitisation up to 14 bit for raw images, resulting in 16,384 grey levels, so that theoretically $10.43\,\mathrm{m}^2\,\mathrm{m}^{-2}$ can be retrieved. Therefore, a higher signal bit depth improves the sensitivity to high LAI as well as maximum retrievable LAI. In the case of the field experiment, the maximum summer PAI was $6\,\mathrm{m}^2\,\mathrm{m}^{-2}$ (Figure 5), which was within the theoretical range.

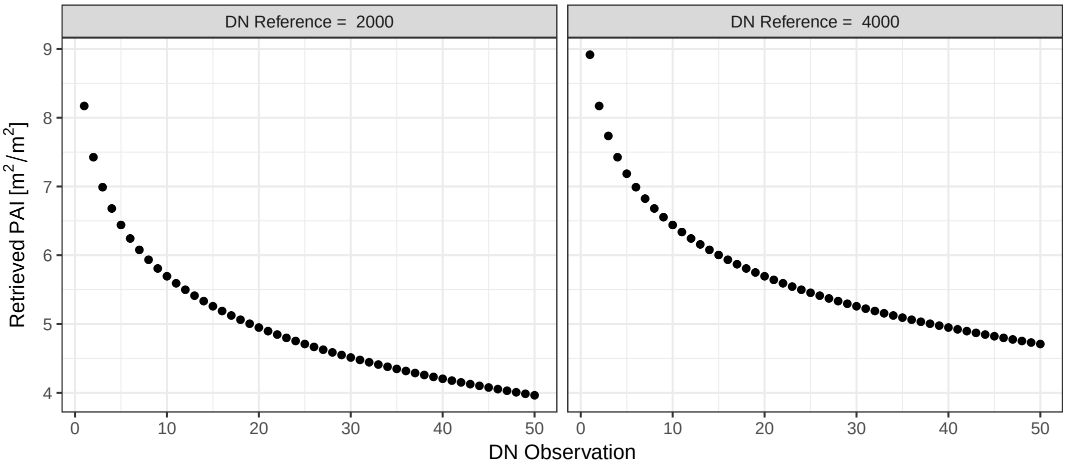

Figure 9. Sensitivity of PASTiS-57 PAI due to digitisation at low observation readings (DN) for two levels of reference readings.

The RTM experiments confirmed the principles underlying the retrievals. In particular, below canopy transmittance measurements in blue and red spectral bands have a high sensitivity to canopy structure and are robust against variation in biochemical composition and illumination conditions. This is not the case for top of canopy reflectance measuring sensors, e.g., tower based or satellite sensors, which often exploit the NIR. These are much more dependent on C_{ab} and illumination angle [28].

However, heterogeneous scenarios confirmed the strong effect of canopy non-randomness on LAI estimation. In particular in case of low tree density scenarios, which violate the homogeneous canopy assumption more than dense canopies with closed cover, LAI was strongly underestimated. Clumping correction after Lang and Xiang [44] counteracted this effect somewhat. Other clumping correction strategies exist, but these usually require estimation of gap size distribution [41,56]. This is possible with DHP, but not with pointing devices, such as PASTiS-57. Therefore, a strategy for field measurements would be to employ multiple PASTiS-57 instruments per plot. Alternatively, a new sensor design based on low-cost micro-computers equipped with fish-eye cameras could be tested. Such an imaging sensor could also retrieve LAD concurrently with LAI [18].

Another disadvantage of the single-band, pointing device design of the PASTiS-57 is the lack of options to distinguish woody and foliage canopy elements. Gower et al. [57] list ranges of 7% to 34% of wood area index contribution to PAI based on a literature review. Previous studies proposed solutions to this problem with multi-band imaging sensors, including NIR [58] or imaging sensors combined with radiative transfer modelling [40]. Another way is multi-temporal estimation by using the winter measured PAI as branch area index and subtract it from the summer measured PAI. However, this neglects radiative interaction processes when both elements are present in the canopy (e.g., occlusion of leaves by branches) and is not agreed on [59]. The lack of consolidated correction methods has also led to a prevalent neglect of correction [40,59]. This topic needs to be addressed with dedicated devices, e.g., dual-wavelength lidar [60].

In the context of sensor simulation, DART proved to be a versatile tool. Especially the option to simulate arbitrary sensors allowed the implementation of the PASTiS-57 sensor in this study. Although sensor simulation with RTMs is not new, below canopy sensor simulations have been restricted to DHP [56] or TLS [61,62]. Another advantage of DART was the option to simulate heterogeneous canopies, which is crucial for forest radiative transfer modelling.

Next to considerations concerning the retrieval principle, thoughts should be given to practical instrument design choices. For instance, the power supply with batteries is a good choice for remote sites and proved to provide electricity for ~1 year. However, close to field stations constant power could be supplied via the electricity grid or from centrally organised solar cells to prevent power loss and missing observations. A permanent data-link to the logger and upload to cloud servers could help to identify sensor problems and monitor results in real-time. Furthermore, the contamination of the sensors with water, falling leaves or needles, or with insects should be taken care of in a long-term deployment. In sites with substantial understorey, sensors could be deployed at different heights and below understorey plants to sample the vertical profile. In addition, sensors at larger heights might be able to focus on the foliage and prevent large stems to be in the FOV.

In the context of a set-up in larger, permanent sample sites, the representative area of PASTiS-57 should be considered to determine the number of required devices. In this respect, PASTiS-57 is comparable to other below-canopy sensors such as DHP and Licor LAI-2000 that measure τ at the hinge angle. Therefore, the diameter of the measurement area is $2\times$ canopy height/$\tan(57.5^{\circ})$. This results in a diameter of 32 m for a 25 m high canopy, as is the case for Speulderbos. Considering geo-location error of 1 pixel [53] this would be representative for Sentinel-2 10 m resolution bands. However, replicates need to be installed per plot to improve precision in the case of LAI validation [54]. In the case of Sentinel-3—when considering geo-location error—a footprint of 1000 m would need to be covered. Locations should be sampled to account for the site heterogeneity, i.e., number of species, differences in canopy structure and presence/variability of understorey.

Furthermore, low-cost, passive sensors such as PASTiS-57 can be combined with light-independent monitoring. For instance, Culvenor et al. [63] presented a monitoring lidar system that samples the hinge angle, similar to the TLS used in this study. These systems are more cost and maintenance intense, but offer opportunities for inter-comparison and benchmarking, also with traditional manual sampling methods. Such a combination of sensors would offer the option of high precision light-independent sensors for site central areas and low-cost sensors for covering larger areas. This would provide the instrument infrastructure necessary for continuous validation of LSP and LAI products, as required by validation Stage 4 of the GCOS LPV group [54].

5. Conclusions

Robust tracking of the phenological cycle and thereby connected canopy biophysical conditions requires sampling techniques with high temporal resolution. This study assessed the ground-based, autonomous, cost-efficient PASTiS-57 instrument in both field and RTM experiments for its performance in forest SOS, EOS and LAI estimation. The instrument design supported acquisition of yearly time series at up to 1 min raw data resolution with low maintenance effort. The choice of the blue spectral region and a viewing angle of 57.5° was found to be robust for a range of canopy biochemical and illumination conditions, thereby focussing on changes in canopy structure, mainly LAI. However, clumping assessment in irregular canopies was limited by the low number of sensors per instrument and the sensors' pointing measurements. In addition, the restriction to a viewing angle of 57.5° alone does not allow retrieval of LAD together with LAI, as is possible with DHP. Future studies should compare PASTiS-57 with other phenology monitoring devices and develop combinations of instruments as site concepts. Other sensor designs could be tested, e.g., based on imaging sensors.

Author Contributions: B.B. designed and conducted the experiments, and wrote the paper. J.-P.G.-E. and N.L. supported the DART experiments. N.L. implemented the sensor option in DART. F.B. designed and built the PASTiS-57 instrument. J.G.P.W.C., J.V. and M.H. scientifically supported and reviewed the paper.

Funding: This work was carried out as part of the IDEAS+ contract funded by ESA-ESRIN.

Acknowledgments: Data analysis was supported by the Research and User Support (RUS) Service. The RUS Service is funded by the European Commission, managed by the European Space Agency, and operated by CSSI and its partners. The authors thank the Dutch Forestry Service (Staatsbosbeheer) for granting access to the site, and Murat Üçer and Christiaan van der Tol for access to the scaffold tower. The fieldwork design of this study was inspired by the M.Sc. thesis of Tom Schenkels (http://edepot.wur.nl/333531). Further thanks go to Marcello Novani, Alvaro Lau Sarmiento and Mathieu Decuyper for help during the fieldwork.

Conflicts of Interest: The authors declare no conflict of interest.

References

1. Kimball, J. Vegetation Phenology. In *Encyclopedia of Remote Sensing*; Njoku, E.G., Ed.; Encyclopedia of Earth Sciences Series; Springer: New York, NY, USA, 2014; pp. 886–890.
2. Richardson, A.D.; Keenan, T.F.; Migliavacca, M.; Ryu, Y.; Sonnentag, O.; Toomey, M. Climate change, phenology, and phenological control of vegetation feedbacks to the climate system. *Agric. For. Meteorol.* **2013**, *169*, 156–173. [CrossRef]
3. Browning, D.; Karl, J.; Morin, D.; Richardson, A.; Tweedie, C. Phenocams Bridge the Gap between Field and Satellite Observations in an Arid Grassland Ecosystem. *Remote Sens.* **2017**, *9*, 1071. [CrossRef]
4. Keenan, T.F.; Darby, B.; Felts, E.; Sonnentag, O.; Friedl, M.A.; Hufkens, K.; O'Keefe, J.; Klosterman, S.; Munger, J.W.; Toomey, M.; et al. Tracking forest phenology and seasonal physiology using digital repeat photography: A critical assessment. *Ecol. Appl.* **2014**, *24*, 1478–1489. [CrossRef] [PubMed]
5. Richardson, A.D.; Braswell, B.H.; Hollinger, D.Y.; Jenkins, J.P.; Ollinger, S.V. Near-surface remote sensing of spatial and temporal variation in canopy phenology. *Ecol. Appl.* **2009**, *19*, 1417–1428. [CrossRef] [PubMed]
6. Petach, A.R.; Toomey, M.; Aubrecht, D.M.; Richardson, A.D. Monitoring vegetation phenology using an infrared-enabled security camera. *Agric. For. Meteorol.* **2014**, *195–196*, 143–151. [CrossRef]
7. Soudani, K.; Hmimina, G.; Delpierre, N.; Pontailler, J.Y.; Aubinet, M.; Bonal, D.; Caquet, B.; de Grandcourt, A.; Burban, B.; Flechard, C.; et al. Ground-based Network of NDVI measurements for tracking temporal dynamics of canopy structure and vegetation phenology in different biomes. *Remote Sens. Environ.* **2012**, *123*, 234–245. [CrossRef]
8. Balzarolo, M.; Anderson, K.; Nichol, C.; Rossini, M.; Vescovo, L.; Arriga, N.; Wohlfahrt, G.; Calvet, J.C.; Carrara, A.; Cerasoli, S.; et al. Ground-based optical measurements at European flux sites: A review of methods, instruments and current controversies. *Sensors* **2011**, *11*, 7954–7981. [CrossRef] [PubMed]
9. Zhang, X.; Friedl, M.A.; Schaaf, C.B.; Strahler, A.H.; Hodges, J.C.F.; Gao, F.; Reed, B.C.; Huete, A. Monitoring vegetation phenology using MODIS. *Remote Sens. Environ.* **2003**, *84*, 471–475. [CrossRef]
10. Che, M.; Chen, B.; Zhang, H.; Fang, S.; Xu, G.; Lin, X.; Wang, Y. A New Equation for Deriving Vegetation Phenophase from Time Series of Leaf Area Index (LAI) Data. *Remote Sens.* **2014**, *6*, 5650–5670. [CrossRef]
11. Chen, J.; Black, T.A. Defining leaf area index for non-flat leaves. *Plant Cell Environ.* **1992**, *15*, 421–429. [CrossRef]
12. Koetz, B.; Baret, F.; Poilvé, H.; Hill, J. Use of coupled canopy structure dynamic and radiative transfer models to estimate biophysical canopy characteristics. *Remote Sens. Environ.* **2005**, *95*, 115–124. [CrossRef]
13. Frampton, W.J.; Dash, J.; Watmough, G.; Milton, E.J. Evaluating the capabilities of Sentinel-2 for quantitative estimation of biophysical variables in vegetation. *ISPRS J. Photogramm. Remote Sens.* **2013**, *82*, 83–92. [CrossRef]
14. Casas, A.; Riaño, D.; Ustin, S.L.; Dennison, P.; Salas, J. Estimation of water-related biochemical and biophysical vegetation properties using multitemporal airborne hyperspectral data and its comparison to MODIS spectral response. *Remote Sens. Environ.* **2014**, *148*, 28–41. [CrossRef]
15. Chianucci, F.; Disperati, L.; Guzzi, D.; Bianchini, D.; Nardino, V.; Lastri, C.; Rindinella, A.; Corona, P. Estimation of canopy attributes in beech forests using true colour digital images from a small fixed-wing UAV. *Int. J. Appl. Earth Obs. Geoinf.* **2016**, *47*, 60–68. [CrossRef]
16. Roosjen, P.P.; Brede, B.; Suomalainen, J.M.; Bartholomeus, H.M.; Kooistra, L.; Clevers, J.G. Improved estimation of leaf area index and leaf chlorophyll content of a potato crop using multi-angle spectral data–potential of unmanned aerial vehicle imagery. *Int. J. Appl. Earth Obs. Geoinf.* **2018**, *66*, 14–26. [CrossRef]
17. Jonckheere, I.; Fleck, S.; Nackaerts, K.; Muys, B.; Coppin, P.; Weiss, M.; Baret, F. Review of methods for in situ leaf area index determination Part I. Theories, sensors and hemispherical photography. *Agric. For. Meteorol.* **2004**, *121*, 19–35. [CrossRef]

18. Weiss, M.; Baret, F.; Smith, G.J.; Jonckheere, I.; Coppin, P. Review of methods for in situ leaf area index (LAI) determination Part II. Estimation of LAI, errors and sampling. *Agric. For. Meteorol.* **2004**, *121*, 37–53. [CrossRef]
19. Lukasová, V.; Lang, M.; Škvarenina, J. Seasonal Changes in NDVI in Relation to Phenological Phases, LAI and PAI of Beech Forests. *Balt. For.* **2014**, *20*, 248–262.
20. Lang, M.; Nilson, T.; Kuusk, A.; Pisek, J.; Korhonen, L.; Uri, V. Digital photography for tracking the phenology of an evergreen conifer stand. *Agric. For. Meteorol.* **2017**, *246*, 15–21. [CrossRef]
21. Berger, M.; Moreno, J.; Johannessen, J.A.; Levelt, P.F.; Hanssen, R.F. ESA's sentinel missions in support of Earth system science. *Remote Sens. Environ.* **2012**, *120*, 84–90. [CrossRef]
22. Donlon, C.; Berruti, B.; Buongiorno, A.; Ferreira, M.H.; Féménias, P.; Frerick, J.; Goryl, P.; Klein, U.; Laur, H.; Mavrocordatos, C.; et al. The Global Monitoring for Environment and Security (GMES) Sentinel-3 mission. *Remote Sens. Environ.* **2012**, *120*, 37–57. [CrossRef]
23. Simic, A.; Baret, F.; Weiss, M.; Lecerf, R.; Alessandrini, A.; Hanocq, J.F.; Marloie, O. Production of the high resolution maps of biophysical variables based on SPOT imagery and in-situ measurements generated by PASTIS 57 for Hyytiala, Finland. In Proceedings of the IEEE International Geoscience and Remote Sensing Symposium, Munich, Germany, 22–27 July 2012; pp. 7655–7658.
24. Raymaekers, D.; Garcia, A.; Di Bella, C.; Beget, M.; Llavallol, C.; Oricchio, P.; Straschnoy, J.; Weiss, M.; Baret, F. SPOT-VEGETATION GEOV1 biophysical parameters in semi-arid agro-ecosystems. *Int. J. Remote Sens.* **2014**, *35*, 2534–2547. [CrossRef]
25. Latorre, C.; Camacho, F.; De la Cruz, F.; Lacaze, R.; Weiss, M.; Baret, F. Seasonal monitoring of FAPAR over the Barrax cropland site in Spain, in support of the validation of PROBA-V products at 333 m. In Proceedings of the 4th International Symposium on Recent Advances in Quantitative Remote Sensing, Torrent, Spain, 22–26 September 2014; pp. 1–6.
26. Nestola, E.; Sánchez-Zapero, J.; Latorre, C.; Mazzenga, F.; Matteucci, G.; Calfapietra, C.; Camacho, F. Validation of PROBA-V GEOV1 and MODIS C5 & C6 fAPAR products in a deciduous beech forest site in Italy. *Remote Sens.* **2017**, *9*, 126.
27. Fang, H.; Ye, Y.; Liu, W.; Wei, S.; Ma, L. Continuous estimation of canopy leaf area index (LAI) and clumping index over broadleaf crop fields: An investigation of the PASTIS-57 instrument and smartphone applications. *Agric. For. Meteorol.* **2018**, *253–254*, 48–61. [CrossRef]
28. Jacquemoud, S.; Verhoef, W.; Baret, F.; Bacour, C.; Zarco-Tejada, P.J.; Asner, G.P.; François, C.; Ustin, S.L. PROSPECT + SAIL models: A review of use for vegetation characterization. *Remote Sens. Environ.* **2009**, *113*, S56–S66. [CrossRef]
29. Clevers, J.G.P.W.; Verhoef, W. LAI estimation by means of the WDVI: A sensitivity analysis with a combined PROSPECT-SAIL model. *Remote Sens. Rev.* **1993**, *7*, 43–64. [CrossRef]
30. Atzberger, C.; Richter, K. Spatially constrained inversion of radiative transfer models for improved LAI mapping from future Sentinel-2 imagery. *Remote Sens. Environ.* **2012**, *120*, 208–218. [CrossRef]
31. Rivera, J.P.; Verrelst, J.; Leonenko, G.; Moreno, J. Multiple cost functions and regularization options for improved retrieval of leaf chlorophyll content and LAI through inversion of the PROSAIL model. *Remote Sens.* **2013**, *5*, 3280–3304. [CrossRef]
32. Campos-Taberner, M.; García-Haro, F.J.; Camps-Valls, G.; Grau-Muedra, G.; Nutini, F.; Crema, A.; Boschetti, M. Multitemporal and multiresolution leaf area index retrieval for operational local rice crop monitoring. *Remote Sens. Environ.* **2016**, *187*, 102–118. [CrossRef]
33. Gastellu-Etchegorry, J.P.; Demarez, V.; Pinel, V.; Zagolski, F. Modeling radiative transfer in heterogeneous 3-D vegetation canopies. *Remote Sens. Environ.* **1996**, *58*, 131–156. [CrossRef]
34. Demarez, V.; Gastellu-Etchegorry, J. A Modeling Approach for Studying Forest Chlorophyll Content. *Remote Sens. Environ.* **2000**, *71*, 226–238. [CrossRef]
35. Banskota, A.; Serbin, S.P.; Wynne, R.H.; Thomas, V.A.; Falkowski, M.J.; Kayastha, N.; Gastellu-Etchegorry, J.P.; Townsend, P.A. An LUT-Based Inversion of DART Model to Estimate Forest LAI from Hyperspectral Data. *IEEE J. Sel. Top. Appl. Earth Obs. Remote Sens.* **2015**, *8*, 3147–3160. [CrossRef]
36. Gastellu-Etchegorry, J.P.; Martin, E.; Gascon, F. DART: A 3D model for simulating satellite images and studying surface radiation budget. *Int. J. Remote Sens.* **2004**, *25*, 73–96. [CrossRef]
37. Gastellu-Etchegorry, J.P.; Lauret, N.; Yin, T.; Landier, L.; Kallel, A.; Malenovsky, Z.; Bitar, A.A.; Aval, J.; Benhmida, S.; Qi, J.; et al. DART: Recent Advances in Remote Sensing Data Modeling With Atmosphere,

Polarization, and Chlorophyll Fluorescence. *IEEE J. Sel. Top. Appl. Earth Obs. Remote Sens.* **2017**, *10*, 2640–2649. [CrossRef]

38. Brede, B.; Bartholomeus, H.; Suomalainen, J.; Clevers, J.; Verbesselt, J.; Herold, M.; Culvenor, D.; Gascon, F. The Speulderbos Fiducial Reference Site for Continuous Monitoring of Forest Biophysical Variables. In Proceedings of the Living Planet Symposium 2016, Prague, Czech Republic, 9–13 May 2016; p. 5.
39. Calders, K.; Schenkels, T.; Bartholomeus, H.; Armston, J.; Verbesselt, J.; Herold, M. Monitoring spring phenology with high temporal resolution terrestrial LiDAR measurements. *Agric. For. Meteorol.* **2015**, *203*, 158–168. [CrossRef]
40. Woodgate, W.; Armston, J.D.; Disney, M.; Jones, S.D.; Suarez, L.; Hill, M.J.; Wilkes, P.; Soto-Berelov, M. Quantifying the impact of woody material on leaf area index estimation from hemispherical photography using 3D canopy simulations. *Agric. For. Meteorol.* **2016**, *226–227*, 1–12. [CrossRef]
41. Leblanc, S.G.; Chen, J.M.; Fernandes, R.; Deering, D.W.; Conley, A. Methodology comparison for canopy structure parameters extraction from digital hemispherical photography in boreal forests. *Agric. For. Meteorol.* **2005**, *129*, 187–207. [CrossRef]
42. Jupp, D.L.B.; Culvenor, D.S.; Lovell, J.L.; Newnham, G.J.; Strahler, A.H.; Woodcock, C.E. Estimating forest LAI profiles and structural parameters using a ground-based laser called 'Echidna'. *Tree Physiol.* **2009**, *29*, 171–181. [CrossRef] [PubMed]
43. Calders, K.; Armston, J.; Newnham, G.; Herold, M.; Goodwin, N. Implications of sensor configuration and topography on vertical plant profiles derived from terrestrial LiDAR. *Agric. For. Meteorol.* **2014**, *194*, 104–117. [CrossRef]
44. Lang, A.; Xiang, Y. Estimation of leaf area index from transmission of direct sunlight in discontinuous canopies. *Agric. For. Meteorol.* **1986**, *37*, 229–243. [CrossRef]
45. Lecerf, R.; Baret, F.; Hanocq, J.; Marloie, O.; Rautiainen, M.; Mottus, M.; Heiskanen, J.; Stenberg, P. *PASTIS 57: Autonomous Light Sensors for PAI Continuous Monitoring. Principles, Calibration and Application to Vegetation Phenology*; AGU Fall Meeting Abstracts 12/2010; American Geophysical Union: Washington, DC, USA, 2010.
46. Hancock, S.; Essery, R.; Reid, T.; Carle, J.; Baxter, R.; Rutter, N.; Huntley, B. Characterising forest gap fraction with terrestrial lidar and photography: An examination of relative limitations. *Agric. For. Meteorol.* **2014**, *189–190*, 105–114. [CrossRef]
47. Calders, K.; Origo, N.; Disney, M.; Nightingale, J.; Woodgate, W.; Armston, J.; Lewis, P. Variability and bias in active and passive ground-based measurements of effective plant, wood and leaf area index. *Agric. For. Meteorol.* **2018**, *252*, 231–240. [CrossRef]
48. Vaccari, S.; van Leeuwen, M.; Calders, K.; Coops, N.C.; Herold, M. Bias in lidar-based canopy gap fraction estimates. *Remote Sens. Lett.* **2013**, *4*, 391–399. [CrossRef]
49. Myneni, R.; Knyazikhin, Y.; Park, T. *MCD15A3H MODIS/Terra+Aqua Leaf Area Index/FPAR 4-Day L4 Global 500 m SIN Grid V006 [Data Set]*; NASA EOSDIS Land Processes DAAC: Sioux Falls, SD, USA, 2015; doi:10.5067/MODIS/MCD15A3H.006.
50. Myneni, R.; Knyazikhin, Y.; Shabanov, N. Leaf Area Index and Fraction of Absorbed PAR Products from Terra and Aqua MODIS Sensors: Analysis, Validation, and Refinement. In *Land Remote Sensing and Global Environmental Change–NASA's Earth Observing System and the Science of ASTER and MODIS*; Ramachandran, B., Justice, C.O., Abrams, M.J., Eds.; Springer: New York, NY, USA; Dordrecht, The Netherlands; Heidelberg, Germany; London, UK, 2011; Chapter 27, pp. 603–633.
51. Bates, D.M.; Watts, D.G. *Nonlinear Regression Analysis and Its Applications*; John Wiley & Sons: New York, NY, USA, 1988; p. 365.
52. R Core Team. *R: A Language and Environment for Statistical Computing*; R Foundation for Statistical Computing: Vienna, Austria, 2014.
53. Drusch, M.; Del Bello, U.; Carlier, S.; Colin, O.; Fernandez, V.; Gascon, F.; Hoersch, B.; Isola, C.; Laberinti, P.; Martimort, P.; et al. Sentinel-2: ESA's Optical High-Resolution Mission for GMES Operational Services. *Remote Sens. Environ.* **2012**, *120*, 25–36. [CrossRef]
54. Fernandes, R.; Plummer, S.; Nightingale, J.; Baret, F.; Camacho, F.; Fang, H.; Garrigues, S.; Gobron, N.; Lang, M.; Lacaze, R.; et al. Global Leaf Area Index Product Validation Good Practices. In *Best Practice for Satellite-Derived Land Product Validation*, 2.0.1 ed.; Schaepman-Strub, G., Román, M., Nickeson, J., Eds.; Land Product Validation Subgroup (WGCV/CEOS): Greenbelt, MD, USA, 2014; p. 76.

55. Jonckheere, I.; Nackaerts, K.; Muys, B.; Coppin, P. Assessment of automatic gap fraction estimation of forests from digital hemispherical photography. *Agric. For. Meteorol.* **2005**, *132*, 96–114. [CrossRef]
56. Gonsamo, A.; Pellikka, P. The computation of foliage clumping index using hemispherical photography. *Agric. For. Meteorol.* **2009**, *149*, 1781–1787. [CrossRef]
57. Gower, S.T.; Kucharik, C.J.; Norman, J.M. Direct and indirect estimation of leaf area index, f(APAR), and net primary production of terrestrial ecosystems. *Remote Sens. Environ.* **1999**, *70*, 29–51. [CrossRef]
58. Kucharik, C.J.; Norman, J.M.; Murdock, L.M.; Gower, S.T. Characterizing canopy nonrandomness with a multiband vegetation imager (MVI). *J. Geophys. Res.* **1997**, *102*, 29455. [CrossRef]
59. Bréda, N.J.J. Ground-based measurements of leaf area index: A review of methods, instruments and current controversies. *J. Exp. Bot.* **2003**, *54*, 2403–2417. [CrossRef] [PubMed]
60. Howe, G.A.; Hewawasam, K.; Douglas, E.S.; Martel, J.; Li, Z.; Strahler, A.; Schaaf, C.; Cook, T.A.; Chakrabarti, S. Capabilities and performance of dual-wavelength Echidna® lidar. *J. Appl. Remote Sens.* **2015**, *9*, 095979. [CrossRef]
61. North, P. Three-dimensional forest light interaction model using a Monte Carlo method. *IEEE Trans. Geosci. Remote Sens.* **1996**, *34*, 946–956. [CrossRef]
62. Grau, E.; Durrieu, S.; Fournier, R.; Gastellu-Etchegorry, J.P.; Yin, T. Estimation of 3D vegetation density with Terrestrial Laser Scanning data using voxels. A sensitivity analysis of influencing parameters. *Remote Sens. Environ.* **2017**, *191*, 373–388. [CrossRef]
63. Culvenor, D.; Newnham, G.; Mellor, A.; Sims, N.; Haywood, A. Automated In-Situ Laser Scanner for Monitoring Forest Leaf Area Index. *Sensors* **2014**, *14*, 14994–15008. [CrossRef] [PubMed]